EES Batteries

ROYAL SOCIETY OF CHEMISTRY

COMMUNICATION

View Article Online
View Journal | View Issue

Cite this: *EES Batteries*, 2025, **1**, 1122

Received 28th April 2025,
Accepted 27th July 2025

DOI: 10.1039/d5eb00080g

rsc.li/EESBatteries

Low temperature polymer electrolyte-based solid-state lithium batteries

Zhiyan Wang,[a,b,c] Hongli Wan*[a,b] and Xiayin Yao *[a,b]

An ultrathin and high-strength solid polymer electrolyte (PPLD) is achieved by employing a polyethylene separator as the skeleton and incorporating a quasi-ionic-liquid for rapid lithium ion transport in poly(vinylidene fluoride-*co*-hexafluoropropene). No significant capacity decay is observed in the $LiFePO_4$/PPLD/Li battery even at −10 °C, indicating its promising potential for low-temperature solid-state lithium batteries.

Broader context

Solid polymer electrolytes have been commercialized due to their significant advantages, including excellent flexibility, low cost and easy production. However, their low ion transport efficiency, poor mechanical properties and insufficient electrolyte/electrode interface stability make it difficult to fully realize their high energy density and safety in solid-state lithium batteries. The thickness and mechanical properties of solid polymer electrolytes can be balanced by integrating a porous polymer framework, while their lithium-ion transport capability and low-temperature performance can also be optimized through specific additives. Herein, we propose a three-dimensional structure solid polymer electrolyte PPLD, where an ultrathin porous polyethylene separator serves as the skeleton, and poly(vinylidene fluoride-*co*-hexafluoropropene) and the $[Li(DMF)_3][TFSI]$ complex are embedded within the pores. The use of an ultrathin PE skeleton effectively reduces the thickness of PPLD while improving its mechanical properties. Furthermore, the incorporated $[Li(DMF)_3][TFSI]$ complex enables rapid lithium-ion migration and superior low-temperature performance. In addition, the evenly distributed poly(vinylidene fluoride-*co*-hexafluoropropene) component facilitates the formation of a robust and stable solid electrolyte interphase film. Fundamentally, this synergistic design combining structural and compositional optimization offers a promising strategy for the development of low-temperature solid-state lithium batteries.

Introduction

Under the advocacy of the green development concept, high-performance energy storage devices, particularly lithium batteries, are encountering numerous challenges, including the need for higher energy density, extended cycle life, enhanced safety and reduced costs.[1–3] Solid-state batteries are considered to be some of the most promising next-generation energy storage devices due to their potentially high energy density and high safety. In solid-state batteries, the lithium metal can serve as the anode and organic liquid electrolytes can be replaced by solid electrolytes.[4–6] As a critical component of a solid-state lithium metal battery, the solid electrolyte plays a decisive role in the overall electrochemical performance of the energy storage device.[7,8] However, the low ion transport efficiency and inferior mechanical properties of the solid electrolyte along with inadequate ion transport dynamics and stability at the electrolyte/electrode interface make it difficult to fully realize their advantages in solid-state lithium batteries.[9,10] Although solid polymer electrolytes (SPEs) have been preliminarily commercialized for use in electric vehicles,[11–14] their poor low-temperature performance, weak mechanical properties and over-thickness require further improvement and optimization.[15,16]

To enhance the low-temperature performance of SPEs, incorporating plasticizer fillers has been demonstrated to be an effective approach.[17] Xu *et al.* proposed a homogeneous ≈150 μm-thick PEO-based SPE with fast ion conduction at a low temperature (0–25 °C) by the addition of succinonitrile.[18] The assembled $LiFePO_4$/Li cell retained a specific discharge capacity of 118.6 mAh g^{-1} after 180 cycles at 0.1 C and 0 °C. Li *et al.* prepared an *N*-dimethylacetamide-based composite

[a]*Ningbo Institute of Materials Technology and Engineering, Chinese Academy of Sciences, Ningbo 315201, P. R. China. E-mail: wanhongli@nimte.ac.cn, yaoxy@nimte.ac.cn*
[b]*Center of Materials Science and Optoelectronics Engineering, University of Chinese Academy of Sciences, Beijing 100049, P. R. China*
[c]*College of Chemistry and Environmental Engineering, Yangtze University, Jingzhou, 434023, P. R. China*

polymer electrolyte using a 1,3,5-trioxane precursor *via in situ* polymerization, enabling fast ion transport and stable cycling at low temperatures.[19] Both the cathode/electrolyte interphase and dual-layered solid electrolyte interphase films can be effectively stabilized by the designed composite polymer electrolyte; thus, the Li/NCM811 pouch cell utilizing this electrolyte presented an initial capacity of 151 mAh g^{-1} at 20 mA g^{-1} and −20 °C. However, the mechanical strength and thickness of SPEs are difficult to improve due to the presence of plasticizers. Generally, superior mechanical properties of SPEs can be achieved by introducing a strong supporting skeleton.[20,21] Zhang *et al.* prepared a cellulose nonwoven supported poly(propylene carbonate)-based SPE with a thickness of about 75 ± 5 μm and a tensile strength of about 25 MPa, which was further applied in ambient temperature $LiFe_{0.2}Mn_{0.8}PO_4$/Li solid-state batteries, showing a capacity retention of up to 96% at 20 °C after 100 cycles.[22] Pazhaniswamy *et al.* synthesized a hybrid poly(vinylidene fluoride) (PVDF)/LiTFSI/Al-LLZO (HPE) solid polymer electrolyte using Al-LLZO ceramic nanofibers as a skeleton *via* electrospinning processes for room-temperature solid-state batteries.[23] The tensile strength and thickness of the HPE solid electrolyte can reach up to 14.88 MPa and 7 μm, respectively. The HPEIC-LFP/Li cell delivers a specific capacity of 159 mAh g^{-1} at 0.5 C after 120 cycles at 25 °C. These works clearly demonstrate significantly enhanced low-temperature performance or mechanical properties of SPEs by introducing plasticizer fillers or supporting skeletons. However, achieving both rapid ion conduction and strong mechanical properties remains a challenge for high-performance SPEs. The balanced overall performance of solid electrolytes in low-temperature batteries influenced by various additives and supporting skeletons still needs to be further explored.

Herein, an ultrathin and high-strength solid polymer electrolyte (PPLD) is achieved by employing a polyethylene (PE) separator as the skeleton and a quasi-ionic liquid for rapid lithium ion transport in the PVDF-based polymer. The PE separator with high porosity (~44%), exceptional mechanical strength and ultra-thin thickness (7 μm) not only endows the PPLD solid electrolyte with superior mechanical properties but also significantly reduces its thickness, thereby shortening the Li^+ migration distance between the cathode and the anode. Moreover, utilizing the strong complexation between dimethylformamide (DMF) and Li^+, the formation of the [Li(DMF)$_3$][TFSI] complex containing $Li^+\cdots O{=}C{-}N$ coordination structures with an appropriate molar ratio leads to high ion conduction efficiency even at low temperatures. In addition, the introduction of a PVDF-based polymer with a high dielectric constant, excellent lithium compatibility and superior electrochemical stability, uniformly embedded in the PE skeleton along with the [Li(DMF)$_3$][TFSI] complex, can effectively guide the uniform distribution of Li^+ during the lithium plating/stripping process and promote the uniform deposition of Li^+. As a result, the PPLD electrolyte demonstrates ionic conductivities up to 1.04×10^{-4}, 1.82×10^{-5} and 9.5×10^{-6} S cm^{-1} at 30, 0 and −10 °C, respectively. Meanwhile, the tensile stress reaches 116.5 MPa with a strain elongation rate of 134.8%. The $LiFePO_4$/PPLD/Li solid-state battery retained 94.7% of its initial specific discharge capacity at 0.5 C over 700 cycles at room temperature. Even at low temperatures of 0 °C and −10 °C, no capacity decay is observed after each 100 cycles, indicating a promising strategy for the design of low temperature solid-state lithium batteries.

Results and discussion

The PPLD solid polymer electrolyte is synthesized by a simple infiltrating and filling method, as shown in Fig. 1a. *N*,*N*-Dimethylformamide (DMF), poly(vinylidene fluoride-*co*-hexafluoropropene) (PVDF-HFP), tetrahydrofuran (THF) and lithium bis(trifluoromethanesulfonyl)imide (LiTFSI) are mixed to form a transparent solution containing a quasi-ionic liquid of [Li(DMF)$_3$][TFSI].[24] Then, the above solution was filled in a 7μm-thick PE separator to obtain the PPLD electrolyte after removing the THF solvent. It is worth noting that the PPLD electrolyte can be easily prepared in a variety of sizes, increasing its practical application feasibility. Fig. 1b shows the SEM image of the PPLD solid polymer electrolyte, exhibiting a dense structure. The slightly wrinkled surface of the PPLD may be due to solvent volatilization during filling and covering of PE by PVDF-HFP and the [Li(DMF)$_3$][TFSI] complex, which does not affect the compatibility and ion conduction at the electrode/electrolyte interface. Additionally, the TGA curve of

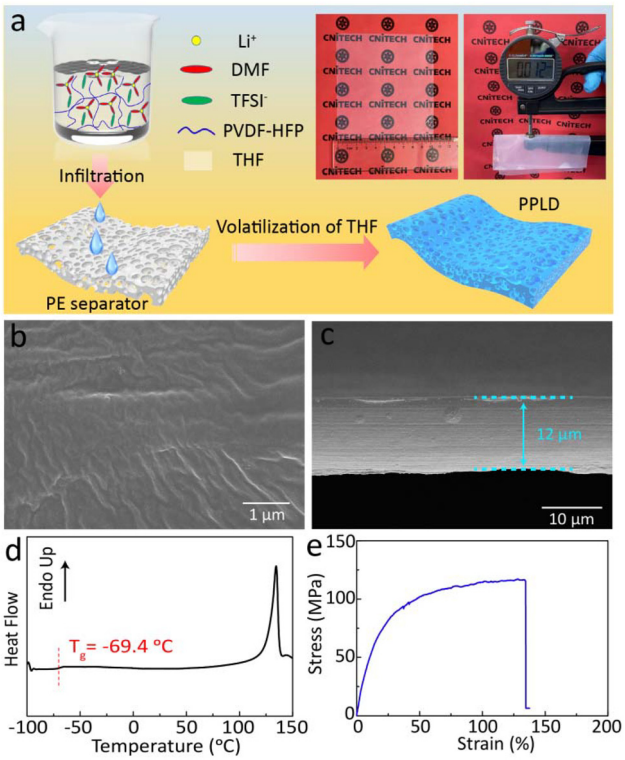

Fig. 1 (a) Schematic illustration of the ultrathin PPLD solid-state electrolyte. (b) Top-view and (c) cross-section SEM images, (d) DSC and (e) stress–strain curves of the PPLD solid-state electrolyte, respectively.

the PPLD solid polymer electrolyte reveals that the DMF content in the PPLD electrolyte is approximately 12.5 wt% (Fig. S1, SI). Notably, the DMF cannot be completely removed until the temperature reaches about 300 °C, which can be attributed to the suppressed activity of DMF due to its interactions with both LiTFSI and the PVDF-based polymer matrix. The thickness of PPLD is determined to be about 12 μm by the cross-section observation (Fig. 1c), which can significantly shorten the lithium ion diffusion pathway and provide sufficient lithium ion conductance. Besides, the DSC curve of the PPLD confirms its glass transition temperature as low as −69.4 °C, ensuring rapid transfer of Li ions in the SPE (Fig. 1d). Moreover, the PPLD solid-state electrolyte possesses high tensile stress up to 116.5 MPa with a strain elongation rate of 134.8% (Fig. 1e), which can not only maintain its own structure during the long-term charge–discharge cycling but also effectively inhibit the growth of lithium dendrites, thus avoiding short circuits in the battery.

The alternating current impedance of the stainless steel/PPLD/stainless steel cell at increasing temperatures ranging from −15 to 30 °C is illustrated in Fig. S2 (SI). The PPLD electrolyte shows high ionic conductivities of up to 1.04×10^{-4}, 1.82×10^{-5} and 9.5×10^{-6} S cm^{-1} at 30, 0 and −10 °C, respectively. In addition, when the temperature decreased to −15 °C, the Nyquist plot of PPLD appeared as a semicircle and its ionic conductivity dropped to 5.78×10^{-5} S cm^{-1}. Moreover, temperature-dependent ionic conductivities of the PPLD solid-state electrolyte also reveal an activation energy E_a as low as 0.4 eV (Fig. 2a), indicating the low transference barrier for lithium ion transport in the PPLD-based cell. Fig. 2b demonstrates that the oxidation stability of the PPLD solid-state electrolyte can reach about 5.3 V due to the ion/dipole–dipole interaction between PVDF-HFP and the [Li(DMF)$_3$][TFSI] complex,[24,25] which will enhance the cycling stability of the assembled battery. In addition, the Li transfer number of the PPLD electrolyte tested by the direct current polarization process was as high as 0.54 (Fig. 2c), which could reduce polarization and inhibit side reactions.

The Li/PPLD/Li battery is assembled to explore the stability of the PPLD solid-state electrolyte against the lithium metal. The galvanostatic voltage profile of the Li/Li symmetric battery at room temperature and step-increased current density is shown in Fig. 2d, and the critical current density is determined to be 0.45 mA cm^{-2}. *In situ* optical microscopy was employed to vividly capture the real-time lithium deposition behavior on the lithium anodes in the Li/liquid electrolyte (LE)/Li cell and the Li/PPLD/Li cell at a current density of 1 mA cm^{-2}, as shown in Fig. S3 (SI) and Fig. 2e, respectively. Initially, the surface of the lithium anode in the Li/LE/Li cell appeared smooth. However, upon lithium deposition for the first 10 minutes, loose dendritic lithium deposits began to form and gradually developed into larger dendritic structures over time. The irregular and rapid growth of these lithium dendrites significantly increases the risk of internal short-circuiting in the battery. In contrast, the ultrathin PPLD electrolyte maintains a nearly constant interfacial distance from the lithium metal electrode throughout the entire deposition process, while increased porosity is observed in the cross-section of the lithium metal, indicating continuous lithium deposition. Neither dendritic growth nor morphological instability is evident at the interface or within the cross-section of the lithium metal. This result confirmed that the PPLD electrolyte can promote uniform lithium deposition and effectively inhibit the growth of lithium dendrites. As shown in Fig. 2f, the Li/PPLD/Li symmetric battery can stably cycle for more than 500 h under 0.1 mA cm^{-2} with a low polarization overpotential of 0.12 V without internal short-circuiting. In addition, the impedance evolution of the Li/PPLD/Li symmetric cell during different storage periods is shown in Fig. S4 (SI). The total resistance gradually increased from ~200 Ω to ~350 Ω over time and eventually stabilized after the fourth day, further confirming the excellent interfacial stability between the PPLD electrolyte and the lithium metal.

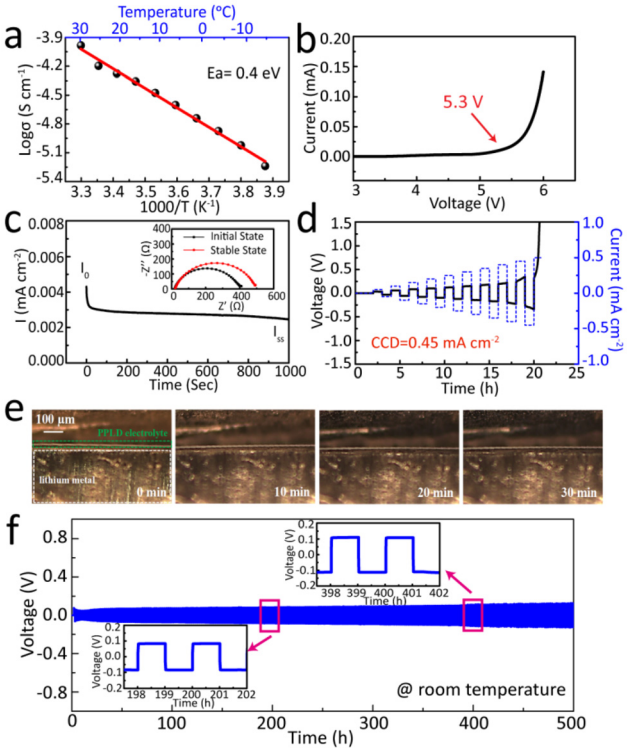

Fig. 2 (a) Temperature-dependent ionic conductivities of the PPLD solid polymer electrolyte. (b) Linear sweep voltammetry curve of the PPLD solid-state electrolyte. (c) Chronoamperometry of the Li/PPLD/Li battery. Inset: the alternating current impedance spectra before and after polarization. (d) Galvanostatic voltage profile of the Li/PPLD/Li battery at step-increased current density. (e) Optical images of the *in situ* Li deposition on the Li/PPLD/Li cell at a deposition current density of 1 mA cm^{-2}. (f) Li/Li symmetric battery with the PPLD solid polymer electrolyte under 0.1 mA cm^{-2}. The insets are voltage profiles of the Li/PPLD/Li battery at 100th and 200th cycles, respectively.

Fig. 3a shows the galvanostatic cycling performance of the LFP/Li battery assembled with the PPLD electrolyte at room temperature. The cell exhibits an initial specific discharge capacity of 143 mAh g^{-1} at 0.5 C and retains 94.7% of its

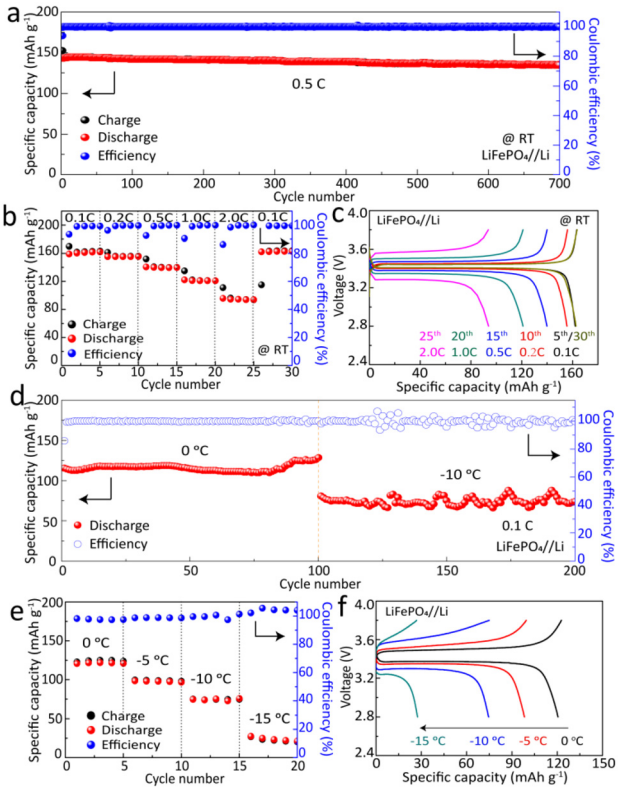

Fig. 3 (a) Cycling stability of the LFP/Li battery assembled with PPLD at 0.5 C at room temperature. (b) Rate performance and (c) voltage profile of the LFP/PPLD/Li battery at different rates at room temperature. (d) Cycling stability of the LFP/PPLD/Li battery at 0.1 C and 0 °C and −10 °C, respectively. (e) Capacity tests of the LFP/PPLD/Li battery at step-decreased temperatures at a 0.1 C rate. (f) Voltage profile of the LFP/PPLD/Li battery at 0.1C and different temperatures.

initial capacity over 700 cycles at room temperature. In addition, the overpotential is almost constant during the 700 cycles (Fig. S5, SI), which is attributed to the excellent electrochemical stability and high ionic conductivity of the PPLD electrolyte. For SPE-based solid-state batteries operating at room temperature, the PPLD electrolyte possesses an ultra-low thickness while maintaining excellent battery performance compared to the reported electrolytes (Fig. S6, SI). In addition, as shown in Fig. 3b and c, the specific discharge capacities are 162.1, 155.6, 140, 121 and 93.9 mAh g^{-1} at 0.1, 0.2, 0.5, 1 and 2 C, respectively. Moreover, when the current density returns to 0.1 C, the specific discharge capacity of the assembled battery can fully recover to approximately 100% of its initial capacity. Excellent reversibility of the PPLD-based cell further highlights the excellent electrochemical stability of the PPLD electrolyte, which can be attributed to the high Li transference number and good ionic transport capability.

Based on the relatively high ionic conductivities and low activation energy of the PPLD electrolyte, the electrochemical performance of the PPLD electrolyte-based LFP/Li solid-state battery is further evaluated at lower temperatures. The long-term cycling performance of the LFP/PPLD/Li battery at 0 °C is demonstrated in Fig. 3d, exhibiting an impressive specific discharge capacity of about 128.5 mAh g^{-1} after 100 cycles at a 0.1 C rate. Moreover, when the temperature drops to −10 °C, the battery still maintains a specific discharge capacity of 78.8 mAh g^{-1} without obvious capacity decay after the subsequent 100 cycles. The LFP/PPLD/Li cell tested at different temperatures (0, −5, −10 and −15 °C) is presented in Fig. 3e and f. Although the specific capacity of the PPLD-based battery drops at lower temperatures due to the increased grain boundary impedance of the PPLD electrolyte (Fig. S2, SI), the battery can still work even if the testing temperature is set as low as −15 °C due to the short ion migration path and low ion transference barrier. The cycling and rate performances of the reported low-temperature LFP/Li batteries are compared in Table S1 (SI), demonstrating that the ultrathin PPLD electrolyte based battery possesses competitiveness in long-term cycling stability and rate performance at low working temperatures.

In addition, the XPS characterization of the cycled lithium metal is employed to reveal the composition of the solid electrolyte interphase film (Fig. 4a). After 100 s of Ar ion sputtering, the C 1s peaks at about 284.8, 286.4 and 290.8 eV correspond to C–C/C–H, C–O and O–C═O, respectively. Besides, the major component LiF after the decomposition of PVDF-HFP chains is observed at about 685 eV in the F 1s spectra.

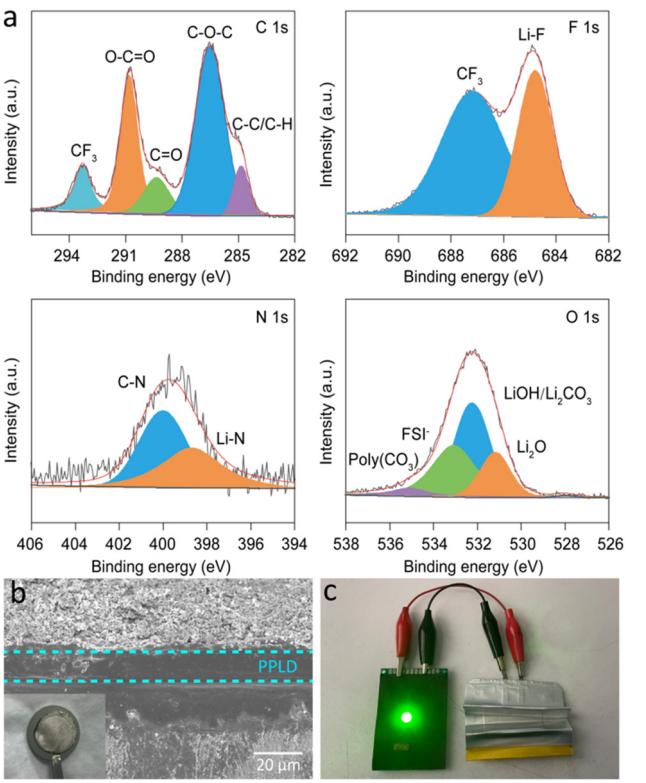

Fig. 4 (a) C 1s, F 1s, N 1s and O 1s XPS spectra of the cycled lithium surface in the LFP/PPLD/Li battery after 100 s Ar sputtering. (b) Cross-section SEM image of the LFP/PPLD/Li battery after each 100 cycles at 0 °C and −10 °C, and the inset is the digital image of the cycled lithium metal surface. (c) Digital image of the flexible LFP/PPLD/Li pouch cell lighting an LED in a repeated folding state.

Moreover, the peaks at about 398.5 eV in the N 1s spectra can be assigned to Li–N after sputtering, which is caused by the decomposition of DMF and $TFSI^-$. In addition, there are also many inorganic components such as $LiOH/Li_2CO_3$ and traces of organic components like poly(CO_3) in the O 1s spectra. Clearly, the LFP/PPLD/Li interface layer mainly consists of abundant LiF/Li–N inorganic species and significant amounts of poly(CO_3) polymeric species, which can stabilize the PPLD|Li interface and promote uniform Li stripping/depositing.[26]

In order to understand the morphological changes of the PPLD electrolyte after long-term cycling at low temperatures, the LFP/PPLD/Li cell cycled at 0 °C and −10 °C is disassembled after 200 cycles. As shown in Fig. 4b, the PPLD electrolyte not only remains intact without decomposition but also preserves its original structure without deformation after 200 cycles at low temperatures, which is inseparable from the synergistic effect of the introduced PE skeleton and the PVDF-HFP polymer matrix. It is also clear that the cycled lithium metal surface still maintains a metallic luster and complete structure, as shown in the inset digital image in Fig. 4b, implying the good compatibility of the PPLD solid-state electrolyte with the lithium metal anode. In addition, the PPLD electrolyte shows excellent flexibility (Fig. S7, SI), and an LED light powered using the flexible LFP/PPLD/Li cell under repeated folding is shown in Fig. 4c. The illumination of the LED remains unaffected by the folded state of the battery, demonstrating the flexibility and reliability of the LFP/PPLD/Li solid-state battery.

Conclusions

In summary, a 12 μm-thick high-strength flexible PPLD solid polymer electrolyte with fast lithium ion conduction at low temperatures is successfully prepared by incorporating a PE separator as the supporting skeleton and a quasi-ionic liquid [Li(DMF)$_3$][TFSI] as the lithium ion conduction medium. Due to the ion/dipole–dipole interaction between PVDF-HFP and the [Li(DMF)$_3$][TFSI] complex, the obtained PPLD solid-state electrolyte exhibits an ultrahigh ionic conductivity of 1.04×10^{-4} S cm^{-1} at 30 °C, excellent oxidation stability and a high lithium transfer number of 0.54. Moreover, the Li/LFP solid-state battery demonstrates stable cycling performance at low temperatures of 0 °C and −10 °C without capacity decay after each 100 cycles, which is inseparable from the dense structure, high mechanical strength, and stable SEI with the lithium metal of the composite PPLD electrolyte, showing great potential of the PPLD solid polymer electrolyte for practical applications in low temperature solid-state lithium batteries.

Experimental section

Lithium bis(trifluoromethanesulfonyl)imide (LiTFSI, 99.95%, Sigma-Aldrich) was mixed with DMF (Aladdin) to prepare LiTFSI/DMF solvates at a molar ratio of 3 : 1. Then, PVDF-HFP (Sigma-Aldrich, M_w = 400 000) and LiTFSI/DMF solvates were dissolved in THF (Aladdin) at 50 °C with a mass ratio of PVDF-HFP to DMF/LiTFSI of 3 : 7. After that, a 7 μm-thick PE separator (SK ENERGY Co., Ltd) was infiltrated with the above solution. Finally, the separator was dried at 40 °C for 24 h to volatilize the residual THF solvent and obtain the resultant electrolyte membrane, abbreviated as PPLD. All experimental procedures above were conducted in an argon-filled glovebox.

The microstructure of the PPLD electrolyte was observed with a Hitachi-S-4800 scanning electron microscope (SEM). The PPLD electrolyte was tested by differential scanning calorimetry using a NETZSCH DSC214 in the range of −100–150 °C, with a heating rate of 10 °C min^{-1} under an N_2 atmosphere. The stress–strain properties of the PPLD electrolyte were characterized using an Instron-3365 instrument. X-ray photoelectron spectroscopy (XPS) was carried out using a PHI5700ESCA instrument.

Electrochemical measurements of the PPLD electrolyte were characterized using the Solartron 1470E multi-channel potentiostat electrochemical workstation. Temperature-dependent ionic conductivities of the PPLD solid polymer electrolyte were measured using the stainless steel (SUS)/SUS cell with a frequency range of 10^6–10 Hz and calculated based on the equation $\sigma = L/(S{\cdot}R)$, in which L is the thickness and R is the bulk resistance of PPLD, respectively, and S presents the effective contacting area between PPLD and SUS. The Arrhenius equation $\sigma(T) = A\exp(-E_a/RT)$ was used to calculate the value of E_a, in which σ, T and A are the ionic conductivity of the electrolyte, the absolute temperature and a pre-exponential factor, respectively. The oxidation stability of the PPLD solid-state electrolyte was recorded using the linear sweep voltammetry (LSV) curves of the SUS/PPLD/Li cell; the sweeping voltage range and constant rate were 3–6 V and 1 mV s^{-1}, respectively. The Li^+ transfer number (t_{Li^+}) of PPLD was tested with a Li/Li symmetric battery by a chronoamperometry test at room temperature, and the applied voltage was 10 mV. t_{Li^+} was calculated using the equation $t_{Li^+} = I_{ss}(\Delta V - I_0R_0)/I_0(\Delta V - I_{ss}R_{ss})$, where ΔV (V) is the applied voltage, I_0 and I_{ss} are the initial and steady-state currents, and R_0 and R_{ss} represent the initial and steady-state resistances of the PPLD electrolyte. In addition, the stability against lithium of the PPLD electrolyte was determined by testing the long cycling performance of Li/Li symmetric batteries at different current densities on a LAND CT-2001A instrument. *In situ* optical microscopy using the YUESCOPE-TD650-RT was employed to capture the real-time lithium deposition behavior on a Li//Li cell assembled with liquid electrolytes (LE, 1 mol L^{-1} $LiPF_6$ dissolved in a mixture of dimethyl carbonate, ethylene carbonate, and ethyl methyl carbonate at a volume ratio of 1 : 1 : 1) and the PPLD solid electrolyte at a current density of 1 mA cm^{-2}.

The $LiFePO_4$ cathode slurry was prepared by mixing $LiFePO_4$, PEO/$LiClO_4$, and super P at a mass ratio of 80 : 10 : 10 in anhydrous acetonitrile. The above slurry was cast onto Al foil and dried at 80 °C overnight under vacuum. The mass loading of $LiFePO_4$ was ~1.5 mg cm^{-2}, and the current rate was set as 1 C = 170 mA g^{-1}. In addition, the thickness of the Li metal (China Energy Lithium Co., Ltd) was about 100 μm. The galvanostatic cycling measurements of the LFP/PPLD/Li

battery were performed on a LAND CT-2001A battery test system within a voltage range of 2.8–3.8 V and at different temperatures, *i.e.* room temperature, 0, −5, −10 and −15 °C.

Author contributions

Zhiyan Wang: investigation, methodology, formal analysis, data curation, validation, visualization, and writing – original draft. Hongli Wan: formal analysis, data curation, validation, and writing – review & editing. Xiayin Yao: conceptualization, supervision, project administration, funding acquisition, resources, and writing – review & editing.

Conflicts of interest

The authors declare that they have no known competing financial interests or personal relationships that could have appeared to influence the work reported in this paper.

Data availability

All data needed to evaluate the conclusions in this paper are present in the main manuscript or its SI.

TG curve of PPLD electrolyte (Fig. S1), alternate current impedance plots of PPLD electrolyte at different temperatures (Fig. S2), optical images of the *in-situ* Li deposition on Li/liquid electrolytes (LE)/Li cell (Fig. S3), interfacial resistances of symmetric Li/PPLD/Li cell with Nyquist plots at various aging times (Fig. S4), voltage profiles of $LiFePO_4$/PPLD/Li pouch cell at different cycles (Fig. S5), thicknesses of reported solid polymer electrolytes and discharge specific capacities of their assembled $LiFePO_4$//Li cells (Fig. S6), digital image of the flexibility of the PPLD electrolyte (Fig. S7), cyclic and rate performances of reported low-temperature $LiFePO_4$//Li batteries assembled with solid polymer electrolytes (Table S1). See DOI: https://doi.org/10.1039/d5eb00080g.

Acknowledgements

This work was supported by the National Key R&D Program of China (grant no. 2022YFB3807700), the National Natural Science Foundation of China (grant no. U21A2075, 52172253, 52102326, 52250610214, 22309194, and 52372244), the Ningbo S&T Innovation 2025 Major Special Programme (Grant No. 2021Z122 and 2023Z106), the Zhejiang Provincial Key R&D Program of China (grant no. 2022C01072 and 2024C01095), the Natural Science Foundation of Hubei Province (grant no. 2025AFB376), the Jiangsu Provincial S&T Innovation Special Programme for Carbon Peak and Carbon Neutrality (grant no. BE2022007), the Baima Lake Laboratory Joint Funds of the Zhejiang Provincial Natural Science Foundation of China (LBMHD24E020001) and the Youth Innovation Promotion Association CAS (Y2021080).

References

1 L. Zhang, S. Wang and Q. Wang, *Adv. Mater.*, 2023, **35**, 2303355.
2 W. Zhang, V. Koverga and S. Liu, *Nat. Energy*, 2024, **9**, 386–400.
3 K. Mu, D. Wang and W. Dong, *Adv. Mater.*, 2023, **35**, 2304686.
4 X. Huang, S. Huang and T. Wang, *Adv. Funct. Mater.*, 2023, **33**, 2300683.
5 Y. Li, X. Wang and H. Zhou, *ACS Energy Lett.*, 2020, **5**, 955–961.
6 X. Lin, C. Chu and Z. Li, *Nano Energy*, 2021, **89**, 106351.
7 L. Tang, B. Chen and Z. Zhang, *Nat. Commun.*, 2023, **14**, 2301.
8 A. Du, H. Lu and S. Liu, *Adv. Energy Mater.*, 2024, **14**, 2400808.
9 D. Wang, H. Xie and Q. Liu, *Angew. Chem., Int. Ed.*, 2023, **62**, e202302767.
10 X. Xie, Z. Wang and S. He, *Angew. Chem., Int. Ed.*, 2023, **62**, e202218229.
11 F. Xu, S. Deng and Q. Guo, *Small Methods*, 2021, **5**, 2100262.
12 J. Jang, J. Ahn and J. Ahn, *Adv. Funct. Mater.*, 2024, **34**, 2470250.
13 O. W. Sheng, C. B. Jin and T. Yang, *Energy Environ. Sci.*, 2023, **16**, 2804–2824.
14 S. Wang, Q. F. Sun and Q. Zhang, *Adv. Energy Mater.*, 2023, **13**, 2204036.
15 K. Yang, L. Chen and J. Ma, *Angew. Chem., Int. Ed.*, 2021, **60**, 24668–24675.
16 Q. Wang, S. Wang and T. T. Lu, *Adv. Sci.*, 2023, **10**, 2205233.
17 L. Z. Fan, H. He and C. W. Nan, *Nat. Rev. Mater.*, 2021, **6**, 1003–1019.
18 S. Xu, Z. Sun and C. Sun, *Adv. Funct. Mater.*, 2020, **30**, 2007172.
19 Z. Li, R. Yu and S. Weng, *Nat. Commun.*, 2023, **14**, 482.
20 J. Y. Wan, J. Xie and X. Kong, *Nat. Nanotechnol.*, 2019, **14**, 705–711.
21 Z. Y. Wang, L. Shen and S. G. Deng, *Adv. Mater.*, 2021, **33**, 2100353.
22 J. Zhang, J. Zhao and L. Yue, *Adv. Energy Mater.*, 2015, **5**, 1501082.
23 S. Pazhaniswamy, S. A. Joshi and H. Hou, *Adv. Energy Mater.*, 2023, **13**, 2202981.
24 L. Chen, T. Gu and J. Mi, *Nat. Commun.*, 2025, **16**, 3517.
25 X. Zhang, S. Wang and C. Xue, *Adv. Mater.*, 2020, **32**, 2000026.
26 H. C. Wang, Q. Wang and X. Cao, *Adv. Mater.*, 2020, **32**, 2001259.